

# Atomistic computer modeling of $[\text{Ru}(\text{bpy})_3]^{2+}$ and $[\text{Ru}(\text{phen})_3]^{2+}$ intercalated into low charged smectites †

Josef Breu,<sup>\*a</sup> Nilesh Raj<sup>b</sup> and C. Richard A. Catlow<sup>b</sup>

<sup>a</sup> *Institut für Anorganische Chemie der Universität Regensburg, D 93040 Regensburg, Germany.*

*E-mail: josef.breu@chemie.uni-regensburg.de*

<sup>b</sup> *Davy Faraday Research Laboratory, 21 Albemarle Street, London, UK W1X 4BS*

*Received 24th November 1998, Accepted 26th January 1999*

Lattice energy minimization techniques have been used to study the 2D molecular organization of  $[\text{Ru}(\text{bpy})_3]^{2+}$  and  $[\text{Ru}(\text{phen})_3]^{2+}$  confined in the interlamellar space of low charged smectites with respect to the stereochemistry of the pillars and the charge distribution within the host. The simulation results underline the complexity of the interplay of long range and short range host–guest and guest–guest interactions in controlling the structure of the interlamellar space. With racemic pillars, favourable  $\pi$  stackings lead to clustering of pillars even with homogeneously charged smectites. Long range and/or short range ordering of the isomorphous substitution within the silicate layer strongly influences the interlayer structure, since host–guest interactions are dominated by electrostatics. The heterogeneity of natural clays rationalises apparently contradicting experimental results on the chiral discrimination by achiral clays.

## Introduction

There is considerable interest in the synthesis of chiral microporous materials for use as stationary phases in separations or as enantioselective heterogeneous catalysts, as such materials may combine good size-, shape-, and stereo-selectivity with various types of catalytic activity.<sup>2–7</sup> In particular, photocatalytic synthesis of chiral compounds has so far only been subjected to limited investigation, because of the lack of photocatalytically efficient metal complexes with high asymmetric induction ability which are not prone to photoracemization or photodecomposition.<sup>8–10</sup> But photochemical reactions in heterogeneous media may differ from analogous reactions in a homogeneous solution due to the restricted geometry of the reaction environment.<sup>11</sup> Construction of highly organized photocatalytic systems is a prerequisite to obtain high efficiency and selectivity.

In principle there are two different routes to arrive at stable chiral inorganic microporous solids. One is the use of chiral templates in the synthesis of framework structures like aluminosilicates or aluminophosphates (ALPOs).<sup>2–7</sup> Such a template synthesis will yield solids with 3D framework structures and it remains to be seen how much of the chiral information is preserved in the framework after the template is removed to generate the microporous solid.

A very promising alternative route is the intercalation of chiral pillars between stable preformed layered solids where microporosity can be controlled *via* the pillar density. Here the 2-dimensionally ordered framework of intercalation hosts is used as a template to control the arrangement and orientation of catalysts and educts in the interlamellar region. Clay materials of the so called 2:1 class, *e.g.* vermiculites or smectites (for nomenclature of clay minerals see Martin *et al.*<sup>12</sup>), distinguish themselves as host materials by the pronounced corrugation of their surfaces, by the rigidity of the layers towards

transverse distortion, and by the tuneability of the charge density of the silicate layers which in turn determines the densities of the cationic pillars.<sup>13,14</sup>

With chiral tris(1,10-phenanthroline)- or tris(2,2'-bipyridyl)-metal complexes ( $[\text{M}(\text{phen})_3]^{n+}$ ,  $[\text{M}(\text{bpy})_3]^{n+}$ ,  $\text{M} = \text{Fe}^{2+}$ ,  $\text{Ru}^{2+}$ ,  $\text{Ni}^{2+}$ ) as guest molecules, remarkable chiral recognition phenomena have been observed. Adsorption capacities, UV/VIS absorption and emission spectra differ depending on whether the complexes are added as a racemic mixture or as a pure enantiomer.<sup>15–20</sup> However, since clay minerals are achiral, there is no simple explanation for the underlying chiral recognition mechanism. Despite this lack of a deeper understanding, clay intercalation compounds (CICs) of optically active  $[\text{Ru}(\text{bpy})_3]^{2+}$  have been used to photooxidize alkyl phenyl sulfides to sulfoxides with an enantiomeric excess of 15–20%.<sup>21</sup> It is expected that the selectivity will increase with our understanding of the complex interplay of host–guest and guest–guest interactions that control the structure of the interlamellar region.

Unfortunately, it is notoriously difficult to ascertain, by direct experiment, the atomic detail of the interlamellar region. Intercalation compounds of natural smectites display turbostratic disorder. In only a very small number of cases of intercalation compounds of the higher charged vermiculites has it been possible to obtain a three-dimensional structure by single crystal X-ray diffraction.<sup>22–25</sup> Even in these cases the interlamellar regions were only partially resolved. For intercalation compounds of smectites even 2D long range order of the interlamellar region is hardly ever observed<sup>26–28</sup> and interpretation of the basal spacing at best indicates the orientation of pillars relative to the silicate sheets.<sup>19,29</sup> Other experimental techniques like absorption, emission,<sup>30–39</sup> Mössbauer,<sup>40,41</sup> and vibrational spectroscopy,<sup>42</sup> NMR,<sup>43</sup> electric dichroism,<sup>29</sup> ESR,<sup>44</sup> and XANES/EXAFS<sup>45</sup> probe the local environment and their structural interpretation is rarely conclusive because of the complexity of the system.

Further progress in this promising field suffers badly from this limited ability to characterize the system experimentally and the consequent lack of a deeper understanding of host–guest and guest–guest interactions controlling the structure of intercalation compounds. This problem is probably the main reason why there is an increasing range of applications of molecular-scale simulations of such compounds using

† Chiral recognition among trisdiimine-metal complexes, Part 4. Part 3; ref. 1. Dedicated to Prof. Dr. K.-J. Range on the occasion of his 60th birthday.

*Supplementary data available:* Tables of potential parameters used. For direct electronic access see <http://www.rsc.org/suppdata/dt/1999/835>, otherwise available from BLDSC (No. SUP 57490, 7 pp.) or the RSC Library. See Instructions for Authors, 1999, Issue 1 (<http://www.rsc.org/dalton>).

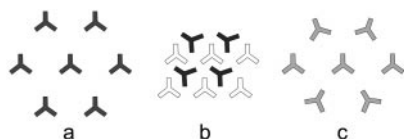


Fig. 1 Schematic representation of possible arrangements of pillars in the interlamellar region of homogeneously charged smectites.

different computational techniques (Monte Carlo, Molecular Dynamics, Lattice Energy Minimizations) and levels of approximation.<sup>1,46–56</sup>

Following our earlier work<sup>1</sup> we have performed atomistic simulations for  $[\text{Ru}(\text{bpy})_3]^{2+}$  and  $[\text{Ru}(\text{phen})_3]^{2+}$  intercalated in trioctahedral smectites with a low layer charge originating from either the tetrahedral layers (saponite,  $[\text{Mg}_3]^{0\text{ct}}[\text{Si}_{3.78}\text{Al}_{0.22}]^{\text{tet}}\text{O}_{10}(\text{OH})_2^{0.22-}$ ) or the octahedral layers (hectorite,  $[\text{Mg}_{2.78}\text{Li}_{0.22}]^{0\text{ct}}[\text{Si}_4]^{\text{tet}}\text{O}_{10}(\text{OH})_2^{0.22-}$ ). With this charge density the complex cation pillars do not use up the available interlamellar space completely. Our main objective was to examine the in-plane structure of the interlamellar region, especially with respect to the given pillar system, stereochemistry of the guest complexes and the charge distribution within the host framework. Using large simulation boxes that contain 8 pillars, it was possible to study different pillar distributions and to probe the relevance of different host–guest and guest–guest interactions to the structure of these intercalation compounds.

## Methodology

### General considerations

Given a uniform charge density of the corrugated clay substrate we can conceive three possible limiting cases for the arrangement of interlayer cations (Fig. 1):

(a) Short-range host–guest interactions are negligible; the guest–guest interactions are dominated by unscreened electrostatic repulsion of the cations, which will consequently arrange in a hexagonal 2-dimensional lattice (Fig. 1a). The lattice constant is a function of the loading and hence of the charge density of the clay which is related to the cation exchange capacity (CEC) because of the charge-neutrality condition. Host lattice and interlamellar structure will only be commensurate for specific loading levels. Experimental support for this model is claimed from adsorptive and diffusive properties of clay systems pillared with  $[\text{Cr}(\text{en})_3]^{3+}$ ,  $[\text{Co}(\text{en})_2]^{3+} - (\text{en})_{1-x}$  (en = ethylenediamine).<sup>28</sup> The formation of this typically incommensurate hexagonal lattice of pillars is also supported by an interpretation of the in-plane XRD peaks of smectites exchanged with  $\text{Ir}(\text{diamsar})^{3+}$ ,  $\text{Hg}(\text{diamsarH}_2)^{4+}$  and  $\text{Hg}(\text{diamsar})^{2+}$  (diamsar = 1,8-diamino-3,6,10,13,16,19-hexaazabicyclo[6.6.6]-icosane).<sup>27</sup>

(b) Again, short range host–guest interactions are negligible. However, attractive lateral interactions between guests are strong enough to induce close-packed islands of interlayer cations despite the electrostatic repulsion. Regardless of the mismatch between non-uniform positive charge density in the interlamellar region and uniform negative charge density in the silicate sheets (Fig. 1b) molecules cluster in the interlamellar region with voids in between. Such oasis/desert scenarios might seem unlikely, but layers of complex cations are a common building block in crystal structures of  $[\text{M}(\text{L}-\text{L})_3]^{2+}$  compounds (L–L = phen, bpy or 4,4'-bipyrimidine).<sup>57–59</sup> Also it is well known that  $[\text{Ru}(\text{phen})_3]^{2+}$  and protonated phen form associates in aqueous solution.<sup>60,61</sup> Furthermore, emission spectra show that (pyrenylbutyl)trimethylammonium tends to cluster on the clay surface and is not adsorbed randomly.<sup>62</sup>

(c) There is a considerable short range host–guest interaction. The molecular recognition between host and guest ensures that the interlamellar structure is always commensurate with the host lattice. Charge neutrality is preserved by creating defects

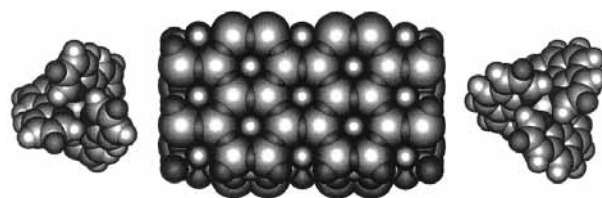


Fig. 2 Match between the arrangement of peripheral hydrogen atoms (dark) of the pillars and the molecular imprinting pattern on the corrugated silicate surface.

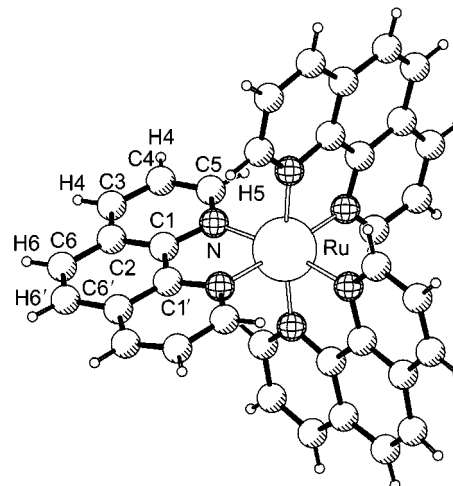


Fig. 3 Labelling scheme used in Table 1.

in the packing of the interlayer cations. The molecular/chiral recognition between guests is altered by the host–guest interaction. Thus the structure of the interlamellar region is determined by both interactions (Fig. 1c).

We have previously performed atomistic simulations of  $[\text{Ru}(\text{bpy})_3]^{2+}$  intercalated in saponite at a loading level high enough to yield a close packed monolayer.<sup>1</sup> The simulation results showed that indeed, for this system, neither host–guest nor guest–guest interactions may be neglected. The delicate molecular imprinting on the silicate surfaces is reinforced by the electrostatic interaction between negative host layers and positive interlayer to the extent that the clay substrate controls the orientations and relative positions of the complex cations in the interlamellar space based on a match between the corrugation of the silicate layer and the shape of the van der Waals surface of the interlayer species (Fig. 2). The lattice energy minima are observed with perfect host–guest fit where all peripheral H atoms that terminate the pillars along their  $C_3$ -axis (H4 in Fig. 3) protrude into hexagonal hollows on the host surface. Given this restriction, the molecular recognition based on lateral guest–guest interactions leads to completely different 2D packing patterns for racemic and enantiomerically pure monolayers of complex cations.

However, at this high loading level the CICs are not microporous. For the design of microporous materials the concentration of the complex cation pillars in the interlamellar region and hence the charge density of the clay has to be reduced. It is therefore crucial to know how changing the clay charge will affect the interlamellar structure. Even under the restriction of a perfect host–guest fit, the key question remains open as to whether short range attractive forces will induce clustering of complex pillars. As outlined above, the interplay of the different host–guest and guest–guest interactions may induce different pillar distributions in the interlamellar space, which in turn determine the size and shape of pores in this microporous material. Therefore the relative energies of clusters of different size and shape need to be compared to an evenly spaced (hexagonal) arrangement of pillars. Since the lateral interactions and consequently the relative strengths of the contributing

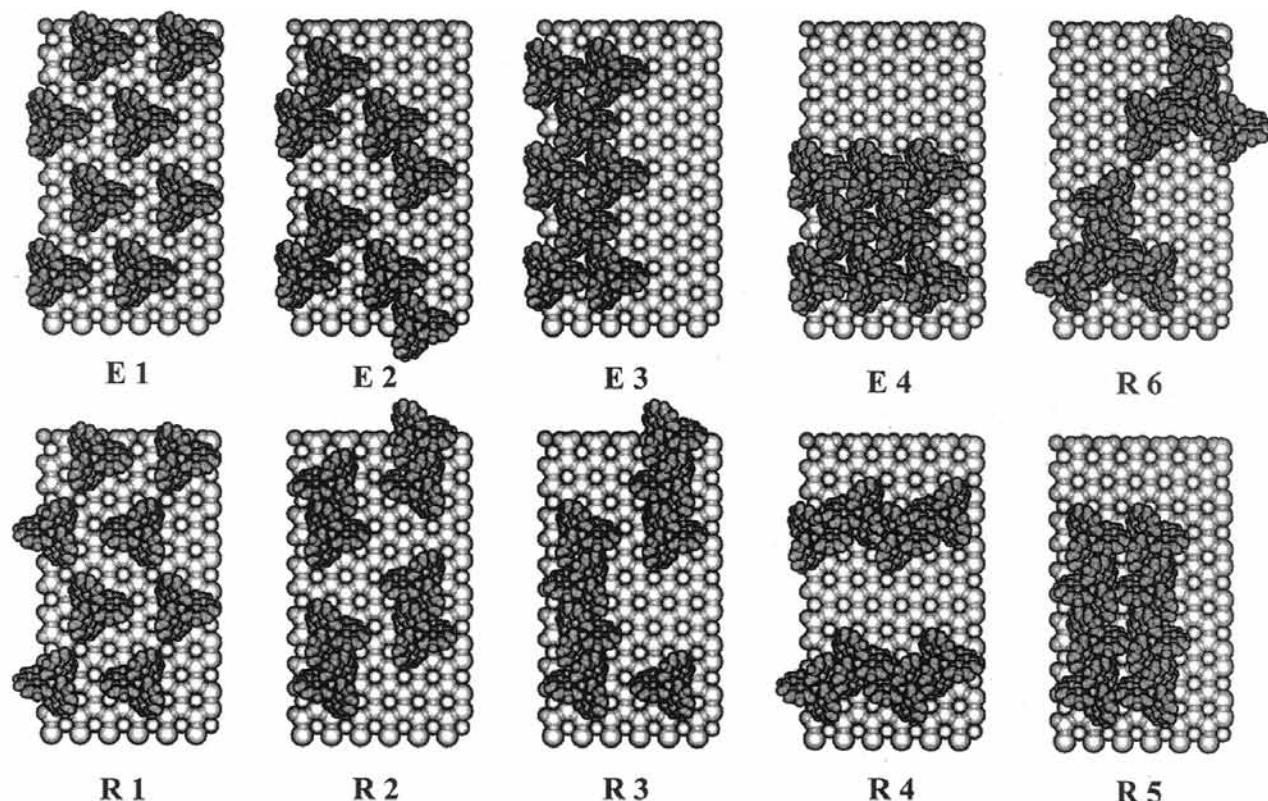


Fig. 4 Local lattice energy minima for different configurations of enantiomeric (E) and racemic (R) pillars confined between homogeneously charged smectite layers.

energy terms vary with respect to the particular pillar system, this problem has to be investigated for different stereochemistries (enantiomeric and racemic) and for the particular ligand system. The results may well be different for  $[\text{Ru}(\text{bpy})_3]^{2+}$  and  $[\text{Ru}(\text{phen})_3]^{2+}$ . It is the aim of this paper to answer these questions using the static lattice atomistic simulation technique which we apply to very large periodic systems.

#### Size of the simulation box and charge density

Regarding the charge density we are somewhat restricted, as in order to be able to use periodic boundary conditions we can only choose those specific loading levels that yield commensurate hexagonal patterns (as in case (a) above). This is the case for a  $2a2b$  supercell of phlogopite with two complex cations and a charge density of 0.5 per formula unit as used in the previous simulation.<sup>1</sup> For the current simulation we are using a lower charge density of 0.22 per formula unit, which corresponds to a  $3a3b$  supercell again with two complex cations. These two charge densities roughly span the range of CECs found for natural smectites. However, with two complexes in the cell, only a dimer can be modeled, therefore we use a yet bigger cell ( $6a6b$ ) with eight complexes in the simulation box. For the starting structures an approximate host–guest fit is provided. Each complex ‘occupies’ three hexagonal hollows on the clay surface. Since only 8 triples out of 72 hollows on each side of the gallery are ‘occupied’, there are thousands of different starting structures. Given the size of the models we had to make sensible choices. Ten representative starting structures with increasing degrees of clustering of pillars were chosen (Fig. 4), which were expected to be energetically favourable and likely to be close to a local minimum based on previous modeling experience<sup>1</sup> and a survey of published packing motifs<sup>57</sup> for this kind of molecular pillar.

#### Computational methods

Probing the energy hypersurface for the ionic, metal-organic/inorganic composite materials under investigation requires a

sound treatment of both long range electrostatic interactions and the short range interactions between guest molecules and between guests and the host lattice. This was achieved in the present study with a classical description of the intracrystalline forces based on the Born model: a covalent ‘molecular mechanics’ potential was used to model the intramolecular forces, while atom–atom pair potentials described the intermolecular interactions.

We continue using the method of static lattice energy minimization with periodic boundary conditions, which takes a starting structure and a set of interatomic potentials, and calculates the structure corresponding to the nearest energy minimum.<sup>46,63–66</sup> This bears the inherent limitation that configurational space has to be sampled by starting from different points; but minimisation methods allow us to model routinely the polarizability of ions in an electric field using a dipolar shell model which has proved crucial to the success in modeling oxide materials.<sup>67</sup> Employing the program GULP,<sup>68</sup> the lattice energy was calculated by standard summation procedures, using the Ewald method<sup>69</sup> for evaluation of the electrostatic term, and real space summation for the short range components of the interaction. The lattice energy was minimized at constant pressure using the Newton–Raphson method starting with a unit Hessian and subsequently updating it with the Broyden–Fletcher–Goldfarb–Shanno algorithm.<sup>70</sup> To ensure that a minimum has indeed been reached, the Rational Function Optimisation<sup>71</sup> was used in the final cycles, which removes imaginary modes from the Hessian, thus forcing it to be positive definite. Temperature is not explicitly considered; the simulations are basically athermal, but some thermal effects may have been subsumed into the interatomic potentials during their fitting to experimental observables.<sup>67</sup>

We should stress that relaxation of the structure was not limited to the pillars, but rather the host framework was fully flexible during the minimization. In particular, the interlayer spacings and the relative shifts of the silicate layers were allowed to alter; hence the shape and size of the unit cell is a variable during minimization.

**Table 1** MEP derived partial charges

	[Ru(bpy) <sub>3</sub> ] <sup>2+</sup>	[Ru(phen) <sub>3</sub> ] <sup>2+</sup>
Ru	0.2828	0.2864
N	-0.1014	-0.1197
C1	0.1366	0.0817
C2	-0.1956	0.1536
C3	0.0079	-0.1414
C4	-0.0664	-0.0654
C5	-0.0819	-0.0567
C6	—	-0.1975
H2	0.1686	—
H3	0.1339	0.1625
H4	0.1430	0.1495
H5	0.1415	0.1360
H6	—	0.1830
rrms (%)	2.8	2.8

For the clay, ionic model potentials with formal charges on Si/Al, Mg/Li and O and a shell model treatment of the polarizability<sup>72</sup> of the oxygen atom were used. Such force fields have been used successfully to model static and dynamic properties of micas as described in detail elsewhere.<sup>63</sup>

The molecular electrostatic potential (MEP) of the complexes was represented by point charges positioned at the nuclei of the atoms. Following a widely used procedure, point charges were fitted to the quantum chemically calculated MEP<sup>73</sup> employing the program POL.<sup>74</sup> The net charge was constrained using a Lagrange multiplier and least squares fits were performed for points given on a rectangular grid (0.2 Å spacing) in a 0.7 Å thick layer outside the van der Waals surface. The charge of the well-buried central atom was fixed to its Hirshfeld partition value<sup>75</sup> and values for symmetry equivalent atoms were averaged. The partial charges listed in Table 1 reproduce the MEP well as indicated by the low rrms values for the fits and should be suited to represent the electrostatic interactions between pillars and between the pillars and host lattice. The MEP was calculated employing the density functional code DMOL.<sup>76,77</sup> Molecular geometries for the single point calculations were taken from published XRD structures with H atoms recalculated at idealized positions (C–H = 1.09 Å) and no symmetry restrictions were applied. We used “DNP” basis sets with inner cores frozen, a “FINE” integration grid, and the Vosko, Wilk, Nusair<sup>78</sup> parameterization of the exchange correlation energy in the homogeneous electron gas. The local approximation was used in SCF iterations and gradient corrections were added in a perturbative approach using the functionals proposed by Perdew and Wang<sup>79</sup> and Becke<sup>80</sup> for the correlation and exchange, respectively.

During lattice energy minimization, the molecular geometry of the complexes was restrained at that found in the crystal structure of β-[Ru(bpy)<sub>3</sub>](PF<sub>6</sub>)<sub>2</sub><sup>81,82</sup> and [Ru(phen)<sub>3</sub>](PF<sub>6</sub>)<sub>2</sub>,<sup>59</sup> respectively, by using strong harmonic potentials between the atoms to fix the bond length and three-body potentials to fix the bond angles. This is well justified in view of the small variations observed for these intramolecular parameters in different crystal environments (e.g. β-[Ru(bpy)<sub>3</sub>](PF<sub>6</sub>)<sub>2</sub>,<sup>81,82</sup> α-[Ru(bpy)<sub>3</sub>](PF<sub>6</sub>)<sub>2</sub>,<sup>83</sup> racemic [Ru(bpy)<sub>3</sub>](ClO<sub>4</sub>)<sub>2</sub>,<sup>84,85</sup> and enantiomeric [Ru(bpy)<sub>3</sub>](ClO<sub>4</sub>)<sub>2</sub><sup>85</sup>). The only molecular parameter that shows significant variation within this series is the torsional angle around the Cl–Cl' bond and realistic energy terms from the cvff-forcefield<sup>86</sup> were used to model torsional motions. We note that force field parameters that are sufficiently reliable and accurate are unavailable for the Ru–N interactions. Since, however, the interactions for the intercalation system are dominated by electrostatic and steric factors, this approach is more adequate for the purpose of this study than introducing uncertainties connected with the intramolecular energetics.

Non-bonding interactions between the complex cations and

both the framework and adjacent complexes are represented using Buckingham potentials fitted by Oie *et al.*<sup>87</sup> to a large range of organic crystal structures. These parameters have been supplemented by Lennard-Jones potentials for the Si–C and Si–H<sub>complex cation</sub> interactions.<sup>88</sup> The cut-off distance for the non-bonding terms was 16 Å. Ru–Ru, Ru–framework, as well as octahedral cation–complex cation interactions were neglected.

### Silicate layer charge models

The permanent negative charge of trioctahedral smectites is generated by isomorphous substitution of higher valent cations by lower valent cations in the octahedral (hectorite) or tetrahedral (saponite) layer. The different cations that occupy a given type of structural site may do so in either a regular or a disordered manner. A truly random distribution is required to meet the definition of a solid solution, which is best represented by a hybrid atom that is statistically part atom A, part atom B. This disordered state seems to be prevalent.<sup>89,90</sup> But there may be also a tendency instead for complete or partial ordering. Long range ordering is indicated in diffraction experiments by lower symmetry or by observation of a superlattice.<sup>91</sup> Ordering may also just occur in small domains. For this short range ordering a second possible ordering scheme, besides symmetry reduction, may be observed, *i.e.* the segregation of isomorphous cations into clusters.<sup>92,93</sup> It has long been known that charge densities in smectites vary from silicate layer to silicate layer in a crystal,<sup>94</sup> but this fundamentally different type of ordering leads to a heterogenous distribution of negative charges within a single silicate layer. The charge density is segregated into low and high density areas. Such short range domains may differ in size, in the nature of the predominant cation and/or the cation ordering.<sup>95</sup>

With a theoretical approach, these different charge distributions at constant CEC can easily be simulated. Computer simulations therefore can provide valuable information on the impact of charge location, charge ordering, and charge distribution on the structure of the interlamellar region. For the main body of the present simulations, a homogeneous saponitic charge distribution using a hybrid species (Al<sub>0.056</sub>Si<sub>0.944</sub>) of charge +3.9444 was used. For selected configurations, additionally a homogeneous hectoritic charge distribution using a (Li<sub>0.074</sub>Mg<sub>0.926</sub>) hybrid species of charge +1.9259 and various ordered and clustered substitution patterns of Al for Si within the tetrahedral layers were studied. Potential parameters for Al in the latter simulations were taken from Gale and Henson.<sup>96</sup>

### Results and discussion

Minimized lattice energies and lattice parameters for different pillar arrangement patterns, pillar systems and host lattice charge models are given in Tables 2–5. All results correspond to the same charge density of the smectite and therefore the same pillar concentration in the interlamellar space. Generally, there is little correlation between density, volume, basal spacing ( $c^\perp$ ) and the total lattice energy of the different components (electrostatic, short range, *etc.*) which contribute to it.

The dimensions of  $a$  and  $b$  deviate little from  $6 \times$  the experimental values found for the related trioctahedral mica phlogopite<sup>97</sup> (5.316(1), 9.221(1) Å) and  $\gamma$  stays close to 90.0°. Even for the clustered arrangements of pillars (e.g. Fig. 8, right) with large voids in between the islands, the rigidity of the silicate layers is correctly represented. Both observations reassure confidence in the forcefield used.

All calculated basal spacings are slightly smaller than the experimental values<sup>19,29</sup> ( $c_{\text{exp}}^\perp = 17.9$  and 17.8 Å for [Ru(bpy)<sub>3</sub>]<sup>2+</sup> and [Ru(phen)<sub>3</sub>]<sup>2+</sup> intercalates, respectively). This trend was already observed in previous simulations<sup>1,63</sup> and is expected for a treatment in which thermal motions are neglected. Since the

**Table 2** [Ru(bpy)<sub>3</sub>]-saponite: calculated energies and structural parameters

Pattern	Enantiomeric intercalate				Racemic intercalate					
	E 1	E 2	E 3	E 4	R 1	R 2	R 3	R 4	R 5	R 6
Total lattice energy/eV	-45509.659	-45508.792	-45506.010	-45499.023	-45509.517	-45509.433	-45508.060	-45508.039	-45503.187	-45508.249
$\Delta E^a/\text{kJ mol}^{-1}$	0	83.65	352.08	1026.23	0	8.10	140.58	142.61	610.76	122.35
$\rho/\text{g cm}^{-3}$	1.700	1.701	1.700	1.707	1.700	1.702	1.703	1.704	1.702	1.702
$\Delta a/\text{\AA}$	3.545	3.546	3.559	3.572	3.542	3.552	3.565	3.537	3.567	3.558
$\Delta b/\text{\AA}$	6.179	6.208	6.241	6.946	6.181	6.234	6.282	6.217	6.270	6.208
$c^*/\text{\AA}$	17.430	17.428	17.432	17.370	17.431	17.421	17.409	17.395	17.419	17.413
$a/\text{\AA}$	32.091	32.091	32.085	32.118	32.091	32.091	32.089	32.091	32.097	32.088
$b/\text{\AA}$	55.637	55.638	55.652	55.582	55.639	55.630	55.634	55.626	55.623	55.635
$c/\text{\AA}$	18.830	18.838	18.855	19.045	18.831	18.841	18.848	18.808	18.853	18.826
$\alpha/\text{^\circ}$	70.84	70.76	70.67	68.61	70.84	70.68	70.53	70.70	70.57	70.74
$\beta/\text{^\circ}$	79.15	79.15	79.12	79.19	79.16	79.13	79.10	79.16	79.09	79.11
$\gamma/\text{^\circ}$	90.00	90.00	90.00	89.99	90.00	90.00	90.00	89.99	89.99	90.00
$V/\text{\AA}^3$	31119.5	31118.1	31127.3	31008.2	31122.9	31100.2	31079.3	31052.4	31098.7	31086.3

<sup>a</sup> Energy relative to the hexagonal patterns E 1 and R 1, respectively.

**Table 3** [Ru(phen)<sub>3</sub>]-saponite: calculated energies and structural parameters

Pattern	Enantiomeric intercalate				Racemic intercalate					
	E 1	E 2	E 3	E 4	R 1	R 2	R 3	R 4	R 5	R 6
Total lattice energy/eV	-45510.242	-45509.873	-45508.041	-45501.380	-45509.893	-45511.032	-45510.643	-45510.631	-45505.841	-45510.286
$\Delta E^a/\text{kJ mol}^{-1}$	0	22.48	173.00	809.72	0	-121.38	-90.41	-94.56	360.09	-54.03
$\rho/\text{g cm}^{-3}$	1.739	1.739	1.738	1.740	1.739	1.740	1.740	1.742	1.739	1.740
$\Delta a/\text{\AA}$	3.546	3.550	3.558	3.551	3.543	3.554	3.564	3.536	3.557	3.557
$\Delta b/\text{\AA}$	6.178	6.196	6.247	6.446	6.176	6.251	6.290	6.179	6.277	6.202
$c^*/\text{\AA}$	17.347	17.349	17.354	17.339	17.349	17.346	17.341	17.325	17.345	17.341
$a/\text{\AA}$	32.092	32.093	32.088	32.116	32.092	32.093	32.091	32.096	32.099	32.091
$b/\text{\AA}$	55.639	55.642	55.655	55.602	55.643	55.635	55.638	55.628	55.631	55.640
$c/\text{\AA}$	18.752	18.762	18.784	18.837	18.753	18.777	18.788	18.731	18.786	18.757
$\alpha/\text{^\circ}$	70.77	70.71	70.58	69.98	70.77	70.55	70.44	70.74	70.48	70.69
$\beta/\text{^\circ}$	79.10	79.09	79.08	79.13	79.11	79.09	79.07	79.12	79.08	79.07
$\gamma/\text{^\circ}$	90.00	90.00	90.00	89.99	90.00	90.00	90.00	89.99	89.99	90.00
$V/\text{\AA}^3$	30973.6	30980.8	30991.8	30962.8	30979.5	30970.6	30962.8	30933.0	30972.5	30961.9

<sup>a</sup> Energy relative to the hexagonal patterns E 1 and R 1, respectively.

**Table 4** [Ru(bpy)<sub>3</sub>]-hectorite: calculated energies and structural parameters

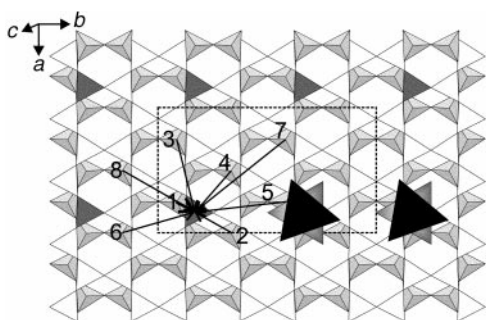
Pattern	Enantiomeric intercalate		Racemic intercalate	
	E 1	E 4	R 1	R 2
Total lattice energy/eV	-45955.636	-45945.190	-45955.488	-45955.422
$\Delta E^a/\text{kJ mol}^{-1}$	0	1007.90	0	6.37
$\rho/\text{g cm}^{-3}$	1.708	1.714	1.708	1.709
$\Delta a/\text{\AA}$	3.540	3.560	3.536	3.544
$\Delta b/\text{\AA}$	6.157	6.928	6.158	6.213
$c^*/\text{\AA}$	17.475	17.415	17.479	17.467
$a/\text{\AA}$	31.982	32.012	31.982	31.983
$b/\text{\AA}$	55.436	55.380	55.438	55.428
$c/\text{\AA}$	18.864	19.077	18.866	18.875
$\alpha^\circ$	70.95	68.704	70.95	70.781
$\beta^\circ$	79.18	79.245	79.20	79.178
$\gamma^\circ$	90.00	89.990	90.00	89.999
$V/\text{\AA}^3$	30983.2	30872.9	30990.1	30965.3

<sup>a</sup> Energy relative to the hexagonal patterns E 1 and R 1, respectively.

**Table 5** [Ru(bpy)<sub>3</sub>]-saponite, different charge models: calculated energies and structural parameters

Pattern	Charge model 1		Charge model 2		Charge model 3	
	E 1	E 4	E 1	E 4	E 1	E 4
Total lattice energy/eV	-45711.816	-45703.842	-45705.972	-45708.774	-45680.866	-45692.701
$\Delta E^a/\text{kJ mol}^{-1}$	0	769.38	0	-270.36	0	-1141.92
$\rho/\text{g cm}^{-3}$	1.708	1.730	1.725	1.709	1.703	1.711
$\Delta a/\text{\AA}$	3.543	3.554	3.580	3.526	3.545	3.507
$\Delta b/\text{\AA}$	6.167	9.464	-0.014	6.050	5.858	6.114
$c^*/\text{\AA}$	17.420	17.195	17.250	17.396	17.460	17.371
$a/\text{\AA}$	32.027	32.023	32.032	32.036	32.046	32.038
$b/\text{\AA}$	55.518	55.509	55.491	55.520	55.507	55.541
$c/\text{\AA}$	18.816	19.947	17.617	18.752	18.755	18.747
$\alpha^\circ$	70.87	61.67	90.04	71.18	70.96	70.96
$\beta^\circ$	79.15	79.74	78.27	79.16	79.10	79.22
$\gamma^\circ$	90.01	89.99	90.00	90.01	89.99	89.98
$V/\text{\AA}^3$	30973.2	30566.0	30660.5	30940.6	31057.2	30909.8

<sup>a</sup> Energy relative to the hexagonal patterns E 1.

**Fig. 5** Different stacking vectors providing the desired host-guest fit for a 2a2b supercell.

bonding in the clay layers is much stronger than that perpendicular to it,  $c_{\text{exp}}^\perp$  will increase more with temperature than will  $a$  and  $b$ .

### Influence of layer stacking faults

Our simulation assumes a perfect crystal while CICs exhibit a wide variety of ordered, partially ordered and fully randomized  $c$  axis stacking arrangements with the latter being predominant. Fig. 5 schematically depicts this stacking fault problem for the racemic monolayer previously identified as the global minimum at high loading level<sup>1</sup> (2 cations per 2a2b supercell). Upper (white/dark gray) and lower (shaded) tetrahedral layers belonging to the same silicate layer are shown. The relative positions of the six peripheral hydrogen atoms (H4 in Fig. 3) of each pillar are an extension of the coordination sphere; they are arranged in two trigonal planes (large shaded and black tri-

angles), which in turn form a trigonal distorted octahedron. Complex cations (only 2 represented) are located above all dark gray tetrahedra and the three lower peripheral H atoms (shaded triangles) of each pillar protrude into three hollows on the upper tetrahedral layer. Note that the black triangles representing the upper three peripheral H atoms of the pillars are not located above the hexagonal hollows of the lower tetrahedral layer. Therefore an orthogonal stacking of consecutive silicate layers would not provide the same host-guest fit for the upper three peripheral H atoms. Rather, the next silicate layer bordering the interlamellar space along  $c^*$  has to be shifted to provide the same host-guest fit for the upper three peripheral H atoms. However, many possible stacking vectors match this requirement; for this small 2a2b simulation box, there are 8 alternative stacking vectors (Fig. 5) which manifest themselves in different triclinic simulation cells (Table 6).

Because of the pseudohexagonal symmetry of the host lattice and its smaller repeat distance, the relative arrangements of consecutive layers and of host lattice and pillars do not change for the different stackings. Dissimilar shifts rather imply discrete mutual alignments of the complex cation monolayers in successive interlayers. Despite the contrasting shift vectors the lattice energies are in fact the same (Table 6). The interaction of guest species in different interlayers is too weak to affect the lattice energy and the minima for the 2D arrangement of interlamellar species will not be perturbed by the long range ordering along the stacking direction and any arbitrarily chosen stacking vector.

On the other hand, this result implies that for this intercalation system, one would not expect 3D ordering as observed for some vermiculite intercalates with much shorter  $c$ -stacking

**Table 6** Influence of different stackings on the lattice energy

	$\Delta a/\text{\AA}$	$\Delta b/\text{\AA}$	$c^\dagger$	$a/\text{\AA}$	$b/\text{\AA}$	$c/\text{\AA}$	$a/^\circ$	$\beta/^\circ$	$\gamma/^\circ$	$E_{\text{Lat.}}/\text{eV}$
1:	0.866	1.450	17.343	10.727	18.597	17.425	85.2	87.2	90.0	-4961.469
2:	-1.816	-3.197	17.335	10.727	18.596	17.721	100.4	95.9	90.0	-4961.482
3:	6.236	1.456	17.342	10.727	18.597	18.487	85.5	70.3	90.0	-4961.469
4:	3.547	-3.191	17.335	10.727	18.596	17.980	100.2	78.6	90.0	-4961.483
5:	0.866	-7.850	17.339	10.728	18.596	19.053	114.3	87.4	90.0	-4961.474
6:	-1.813	6.112	17.339	10.728	18.595	18.474	70.7	95.6	90.0	-4961.475
7:	6.233	-7.852	17.338	10.727	18.597	20.028	113.1	71.9	90.0	-4961.476
8: <sup>a</sup>	3.550	6.113	17.338	10.727	18.596	18.724	70.9	79.1	90.0	-4961.480

<sup>a</sup> Stacking vector used in previous<sup>1</sup> and this work.

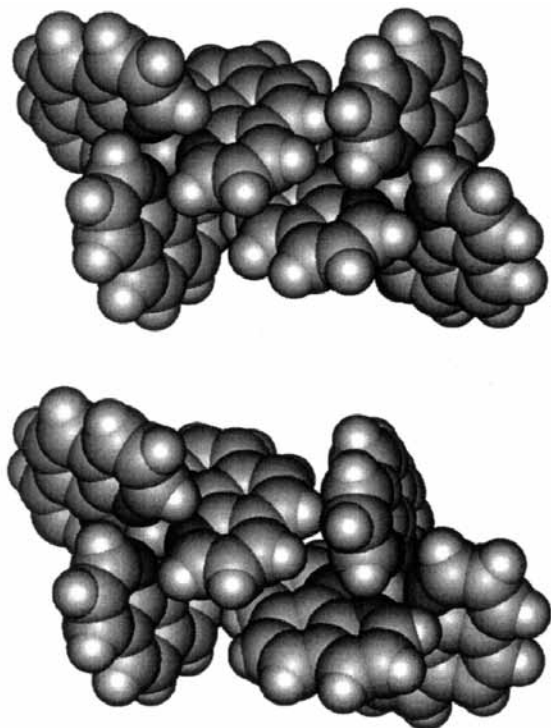


**Fig. 6** Shifted  $\pi$ -stacking arrangements between aromatic ligands of neighbouring cations as observed in  $[\text{Ru}(\text{phen})_3](\text{PF}_6)_2$ <sup>59</sup> (bottom) and in the lattice energy minimum for pattern R4 (top).

distances.<sup>22–25</sup> The favourable host–guest interaction bridging the interlamellar space might induce fixed phase relationships for the host layers, but guest ordering will only be two-dimensional.

#### Distribution of pillars in the interlamellar space

With  $[\text{Ru}(\text{bpy})_3]^{2+}$  intercalated into a homogeneously charged saponite (Table 2) the energy minimum for both enantiomeric and racemic interlayers is observed with the hexagonal arrangement of pillars (E 1 and R 1).

Due to the large electrostatic repulsion in E 4, the cationic pillars move a little further apart along  $b$  with Ru–Ru distances increasing from 10.7 to 11.0–11.3  $\text{\AA}$  in this direction during minimization. As a consequence, 6 out of 48 peripheral H atoms are forced out of the hexagonal hollows on the clay substrate in the local minimum of E 4. However, despite large energy differences for some configurations, all other local minima are observed with perfect host–guest fit emphasizing the importance of short range host–guest interactions with this intercalation system.

Surprisingly, the picture changes when switching to the supposedly very similar pillar  $[\text{Ru}(\text{phen})_3]^{2+}$ . Here, for enantiomeric interlayers, E 1 is still energetically favoured over any clusters investigated (Table 3). However, with racemic intercalates, shifted  $\pi$  stacks can be realized between aromatic

ligands of neighbouring cations. This intermolecular packing pattern is also observed for  $[\text{Ru}(\text{phen})_3](\text{PF}_6)_2$ <sup>59</sup> (Fig. 6). As a consequence of chirality this penetration of two complexes with parallel  $C_3$ -axes, as required by the host–guest interaction, is only feasible with a racemic pair. Note the structure directing effect of the peculiar anion clay, which forces the  $C_3$ -axis to be exactly parallel, while in  $[\text{Ru}(\text{phen})_3](\text{PF}_6)_2$  they are slightly tilted. Owing to the inherent polarity of aromatic systems, the electron rich core being surrounded by an electron poor torus of H atoms, this is a favourable ' $\pi$ - $\pi$ -interaction'.<sup>98</sup> Lateral interactions of this kind are popular motifs in crystal packings of aromatic compounds<sup>99,100</sup> and their general importance in molecular recognition has been acknowledged.<sup>101,102</sup> Apparently with the cation–cation distances and orientations induced by the clay surface corrugation, this interaction is stronger for the larger  $\pi$  system (phen as compared to bpy) and even large clusters like one dimensional chains of complex cations running along  $a$  (R 4) are lower in energy than the hexagonal pattern (R 1). These results suggest that racemic  $[\text{Ru}(\text{phen})_3]^{2+}$  will cluster in the interlamellar space of saponites even if the host layer charge density is homogeneous.

Admittedly, the energy differences are relatively small and raise the question of significance. While it is difficult to quantify precisely the uncertainties associated with the interatomic potentials, the errors associated with computational and numerical aspects (*e.g.* cutoffs in summations) are low (<1 kJ mol<sup>-1</sup>). We consider that these will not influence the main conclusions drawn from our results.

Interestingly, enantiomeric and racemic hexagonal patterns differ already in lattice energy. The central atoms in these configurations are still 16  $\text{\AA}$  apart, but the molecules already sense their MEP and the cooperative long-range electrostatic interaction for this structure is in favour of the enantiomers (by 14.67 and 35.51 kJ mol<sup>-1</sup> for  $[\text{Ru}(\text{bpy})_3]^{2+}$  and  $[\text{Ru}(\text{phen})_3]^{2+}$ , respectively).

Moving the origin of the permanent silicate charge from the tetrahedral to the octahedral layer and hence further away from the interlayer cations alters the relative weight of host–guest and guest–guest interactions (Table 4), which makes clustering more feasible. The difference between E 4 and E 1 declines from 1026.26 to 1007.90 kJ mol<sup>-1</sup> when going from saponite to hectorite. Moreover, for the hectorite intercalate, pairs of  $[\text{Ru}(\text{bpy})_3]^{2+}$  (R 2) have energies that are so close to that of the hexagonal arrangement of pillars (R 1) that a change in model ordering cannot be ruled out, especially when we recall that entropy terms are not included in our assessment of the relative stability of different structures. This result emphasizes the complexity of the interplay of long-range and short-range, host–guest and guest–guest interactions in controlling the structure of the interlamellar space. Presumably minor changes in the pillar or host system may completely alter the structure.

#### Influence of the charge distribution within the clay layers

The picture becomes even more complicated and subtly differentiated when taking into account alternative charge distri-

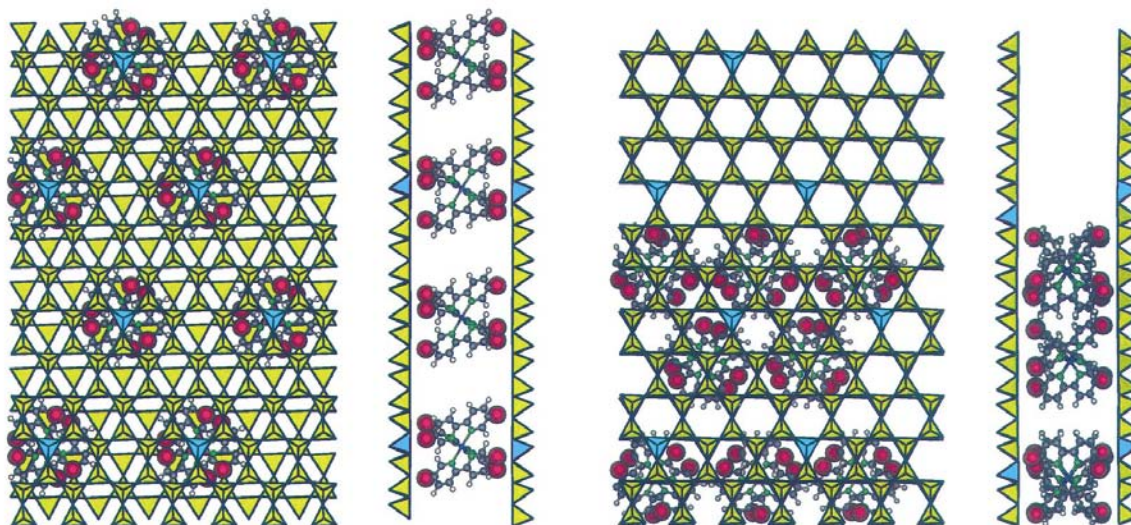


**Fig. 7** Local lattice energy minima for pattern E 1 (left) and E 4 (right) with charge model 1 viewed perpendicular to the silicate layers and along  $a$ . Al-containing tetrahedra are shown in blue. The protruding hydrogen atoms are red and depicted with realistic van der Waals radii.

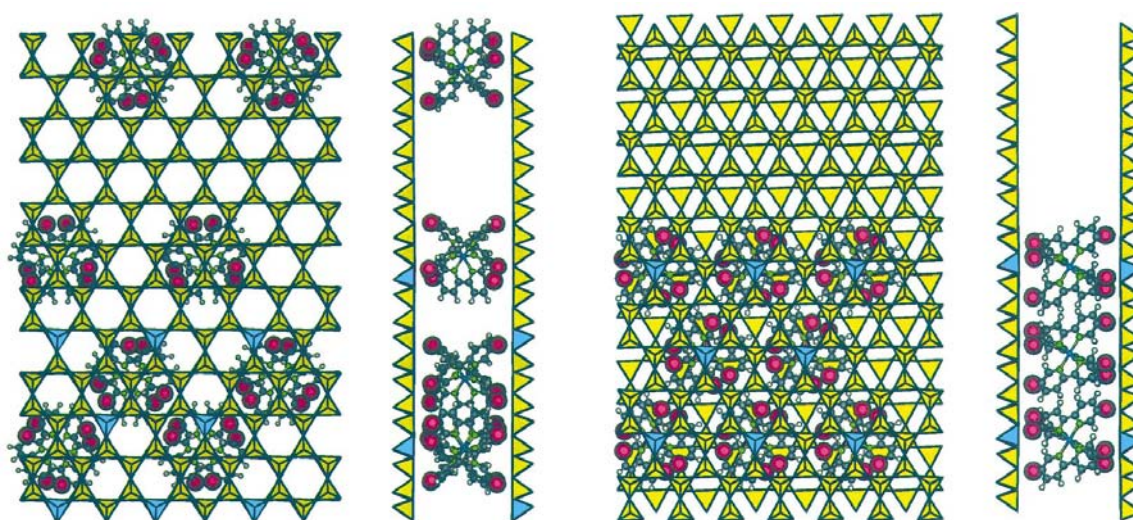


**Fig. 8** Local lattice energy minima for pattern E 1 (left) and E 4 (right) with charge model 2 viewed perpendicular to the silicate layers and along  $a$ . Al-containing tetrahedra are shown in blue. The protruding hydrogen atoms are red and depicted with realistic van der Waals radii.

butions in the host material. We have investigated three different charge models in combination with two starting configurations, E 1 and E 4 (Table 5, Figs. 7–9). For charge model 1, Al was explicitly assigned in a fully ordered hexagonal superlattice (magenta tetrahedra). The substitution pattern follows the pillar locations in configuration E 1. Charge models 2 and 3 represent cases for short range ordering with segregation of isomorphous substitution into higher charged islands. With charge model 2, isomorphous substitution follows the pillar distribution in configuration E 4, while charge model 3 reflects the maximum Löwensteinian clustering of isomorphous substitution.

Starting structures with a prevalent mismatch between the isomorphous substitution pattern in the host and the pillar arrangement in the interlayer (charge model 1/E 4, charge model 2/E 1, and charge model 3/E 1) are far from any local minimum. This expresses itself in substantial changes in shifting vectors and in large displacements of pillars from their initial positions during minimization. This observation gives us some confidence that we have covered configurational space more thoroughly than suggested by the limited selection of starting structures. Clearly, the host–guest interactions are

dominated by the electrostatics and the molecular imprinting manifested in the short-range interactions is overruled. Consequently the host–guest fit for the local minima identified for these configurations is not strictly obeyed. The  $C_3$ -axis of some pillars is no longer exactly perpendicular to the silicate surface. Surprisingly this tilting does not show in the basal spacings. On the other hand, configurations where pillar arrangement and substitution pattern correspond (charge model 1/E 1, charge model 2/E 4, and charge model 3/E 4) have local minima close to the starting structures. Despite the increased charge clustering, the pillar arrangement does not change any further for the latter as compared to charge model 2/E 4, because short range guest–guest and/or host–guest interactions will not allow any denser packing. The host–guest fit for both is perfect, while the Ru–Ru distances marginally decrease from 10.65–10.75 to 10.47–10.68 Å when going from charge model 2 to charge model 3.

Looking at the relative energies for these ordered systems, several important conclusions can be drawn. As might have been anticipated, interlayer cation distribution will follow any long-range and/or short-range ordering of substitution in the host lattice, because the electrostatic energy is the lead-

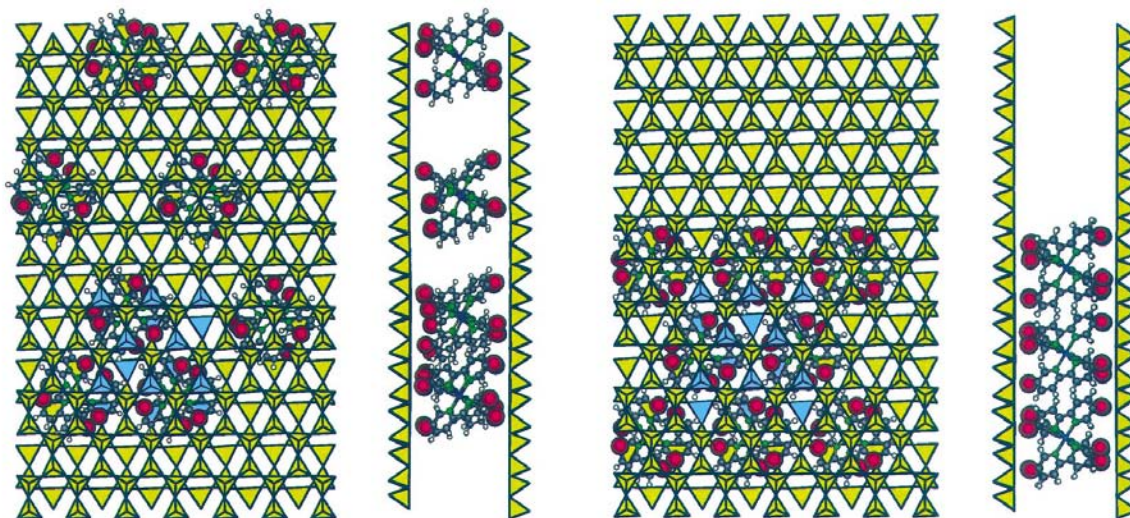


**Fig. 9** Local lattice energy minima for pattern E 1 (left) and E 4 (right) with charge model 3 viewed perpendicular to the silicate layers and along *a*. Al-containing tetrahedra are shown in blue. The protruding hydrogen atoms are red and depicted with realistic van der Waals radii.

ing term in host–guest interactions. Constructing supercells in the manner done with charge model 1 creates highly ordered structures which do not truly represent the solid solution hosts most frequently encountered in nature. Unless there is good reason to assume such an ordering, this approach will introduce severe artefacts and involves the inherent risk to arrive at wrong conclusions regarding the structure of CICs.

On the other hand, the results show convincingly that a heterogeneous distribution of negative charges within the silicate layer as proposed by Muller *et al.*<sup>93</sup> for montmorillonite will inevitably induce clustering of pillars in the interlamellar space. Note that we have deliberately selected the cluster configuration that gave the poorest lattice energy compared to the hexagonal arrangement of pillars between homogeneously charged smectite layers. Still there is a strong energetic preference for pillar clustering with clay charge models 2 and 3.

This result puts the focus back on the importance of charge characterization and charge control of the host system in intercalation chemistry. It will be essential to synthesize monophasic, homogeneously charged host materials in order to be able to construct highly organized intercalation compounds. Even then, lateral interactions between certain pillars might cause a non-uniform pillar distribution.

When working with natural smectites, characterization of exchange properties solely by bulk CECs is insufficient and will make a conclusive interpretation of experimental results and their reproduction difficult. This point can best be illustrated by looking at the many papers published on the luminescence behaviour of  $[\text{Ru}(\text{bpy})_3]^{2+}$  and  $[\text{Ru}(\text{phen})_3]^{2+}$  intercalated in smectites. For example, while Joshi *et al.* found higher emission intensities for  $\Delta, \Lambda$ - $[\text{Ru}(\text{bpy})_2]^{2+*}$  than for the enantiomers, but higher emission intensities for enantiomeric  $[\text{Ru}(\text{phen})_3]^{2+*}$  as compared to the racemates,<sup>18</sup> Shimizu *et al.*<sup>37</sup> report that emission intensities of racemates are higher than for enantiomers for *both* pillar systems. It has been found that self-quenching or concentration quenching readily occurs with increasing loading, indicating that clustering, rather than random distribution of  $[\text{Ru}(\text{bpy})_3]^{2+}$  does occur. Moreover, this clustering is more pronounced for the racemic mixture than for the enantiomers.<sup>30,31,36</sup> Kamat *et al.*<sup>36</sup> have recognized that the spectroscopic differences are based on distinct host–guest and guest–guest interactions. However, their interpretation is inconclusive in view of the lack of an in depth characterization of the charge distribution of the host material used. Therefore it is unclear whether the driving force for clustering was a heterogeneous

charge density of the host or ‘ $\pi$ – $\pi$ -interactions’ between racemic pillars or a combination of both.

Our simulation results, for the first time, rank the different host–guest and guest–guest interactions and offer a firmer base for the interpretation of the experimental observations. In the light of the delicate balancing of different interactions demonstrated for the idealized limiting cases apparently contradicting experimental facts may be rationalised.

## Conclusions

The simulations described in this paper highlight the complexity of the interplay of different host–guest and guest–guest interactions controlling the structure of the interlamellar region. Calculations of the type reported here allow a detailed and accurate treatment of the competing terms and may be used to probe the energetics and structures of such composite materials. On the other hand, this will allow a more conclusive interpretation of experimental data, but on the other hand it will also foster synthetic approaches that lead to materials with improved properties.

Already, supposedly minor changes in host (hectorite *vs.* saponite) or pillar system ( $[\text{Ru}(\text{bpy})_3]^{2+}$  *vs.*  $[\text{Ru}(\text{phen})_3]^{2+}$ ) may result in different pillar arrangement and clustering. Moreover, the corrugation of the host layers may not be neglected. It is essential to allow simultaneous relaxation of both the relative shift of silicate layers and the basal spacing during minimization to develop a realistic picture of the energetics of intercalation chemistry.

In his recent review Schoonheydt states that “all the data taken together show that an adequate explanation for chiral discrimination by chiral clays is not yet available.”<sup>39</sup> We consider that simulations of the type reported here can yield considerable information on the mechanism of the observed chiral recognition phenomena. The results suggest that the clay mineral controls the orientations and relative positions of the complex cations in the interlamellar space based on the match between host and guest shape and the charge density distribution if ordering in the isomorphous substitution pattern is present. From there on, everything is determined by lateral interactions between the chiral pillars. In particular, favourable shifted  $\pi$  stacks can only be realized for racemic pairs. It should be stressed that this interaction leads to different interlamellar structures at the same loading level. For the intercalation systems where clustering is preferred, these differences will occur even at very low loading levels. Even though we did not con-

sider structural quenchers like Fe<sup>3+</sup>, our simulation results offer a satisfactory explanation of published experimental observations, especially in the light of the heterogeneity of natural clays.

## Acknowledgements

We are indebted to the Leibniz-Rechezentrum and the S.E.R.C. for generous allocation of computer time. We are grateful to Dr. J. D. Gale for many useful discussions and code modifications and to G. Fuchs for helping with code implementation. Finally, J. B. would like to thank Prof. K.-J. Range for his constant support and the Fonds der Chemischen Industrie, and the Deutsche Forschungsgemeinschaft for financial support.

## References

- 1 J. Breu and C. R. A. Catlow, *Inorg. Chem.*, 1995, **34**, 4504.
- 2 K. Morgan, G. Gainsford and N. Milestone, *J. Chem. Soc., Dalton Trans.*, 1995, 425.
- 3 D. A. Bruce, A. P. Wilkinson, M. G. White and J. A. Bertrand, *J. Chem. Soc., Dalton Trans.*, 1995, 2059.
- 4 D. A. Bruce, A. P. Wilkinson, M. G. White and J. A. Bertrand, *J. Solid State Chem.*, 1996, **125**, 228.
- 5 J. A. Bertrand, D. A. Bruce, A. P. Wilkinson, P. E. Dai, R. H. Petty and M. G. White, in *Catalysis of Organic Reactions*, ed. R. E. Malz, Marcel-Dekker Inc., New York, 1996.
- 6 M. J. Gray, J. D. Jasper, A. P. Wilkinson and J. C. Hanson, *Chem. Mater.*, 1997, **9**, 976.
- 7 S. M. Stalder and A. P. Wilkinson, *Chem. Mater.*, 1997, **9**, 2168.
- 8 R. M. L. Warren, A. G. Lappin and A. Tatehata, *Inorg. Chem.*, 1992, **31**, 1566.
- 9 K. Ohkubo, M. Fukushima, H. Ohta and S. Usui, *J. Photochem. Photobiol. A: Chem.*, 1996, **98**, 137.
- 10 K. Ohkubo, T. Hamada, H. Ishida, M. Fukushima, M. Watanabe and H. Kobayashi, *J. Chem. Soc., Dalton Trans.*, 1994, 239.
- 11 M. Ogawa and K. Kuroda, *Chem. Rev.*, 1995, **95**, 399.
- 12 R. T. Martin, S. W. Bailey, D. D. Eberl, D. S. Fanning, S. Guggenheim, H. Kodama, D. R. Pevear, J. Środoń and F. J. Wicks, *Clays Clay Miner.*, 1991, **39**, 333.
- 13 S. A. Solin, *Annu. Rev. Mater. Sci.*, 1997, **27**, 89.
- 14 M. F. Thorpe and S. A. Solin, in *Access in Nanoporous Materials*, ed. T. J. Pinnavaia and M. F. Thorpe, Plenum Press, New York, 1995.
- 15 A. Yamagishi and M. Soma, *J. Am. Chem. Soc.*, 1981, **103**, 4640.
- 16 A. Yamagishi, *J. Chem. Soc., Dalton Trans.*, 1986, 290.
- 17 A. Yamagishi, *J. Coord. Chem.*, 1987, **16**, 131.
- 18 V. Joshi, D. Kotkar and P. K. Ghosh, *Proc. Indian Acad. Sci.: Chem. Sci.*, 1990, **102**, 203.
- 19 G. Villemure, *Clays Clay Miner.*, 1991, **39**, 580.
- 20 A. Yamagishi, in *Fundamental and Applied Catalysis*, ed. M. V. Twigg and M. S. Spencer, Plenum Press, New York, 1993.
- 21 T. Hikita, K. Tamaru, A. Yamagishi and T. Iwamoto, *Inorg. Chem.*, 1989, **28**, 2221.
- 22 P. G. Slade and P. A. Stone, *Clays Clay Miner.*, 1984, **32**, 223.
- 23 P. G. Slade, C. Dean, P. K. Schultz and P. G. Self, *Clays Clay Miner.*, 1987, **35**, 177.
- 24 P. G. Slade and P. A. Stone, *Clays Clay Miner.*, 1989, **37**, 81.
- 25 A. Vahedi-Faridi and S. Guggenheim, *Clays Clay Miner.*, 1997, **45**, 859.
- 26 S. A. Solin, in *Chemical Physics of Intercalation II*, ed. J. Bernstein, J. E. Fischer, S. Roth and S. A. Solin, NATO ASI Series B, Plenum Press, New York, 1993.
- 27 F. Tsvetkov and J. White, *J. Am. Chem. Soc.*, 1988, **110**, 3183.
- 28 B. Y. Chen, H. Kim, S. D. Mahanti, T. J. Pinnavaia and Z. X. Cai, *J. Chem. Phys.*, 1994, **100**, 3872.
- 29 M. Taniguchi, A. Yamagishi and T. Iwamoto, *Inorg. Chem.*, 1991, **30**, 2462.
- 30 P. K. Ghosh and A. J. Bard, *J. Phys. Chem.*, 1984, **88**, 5519.
- 31 R. A. Schoonheydt, P. Depauw, D. Vliers and F. C. Deschrijver, *J. Phys. Chem.*, 1984, **88**, 5113.
- 32 V. Joshi, D. Kotkar and P. K. Ghosh, *J. Am. Chem. Soc.*, 1986, **108**, 4650.
- 33 V. Joshi and P. K. Ghosh, *J. Chem. Soc., Dalton Trans.*, 1987, 789.
- 34 V. Joshi, D. Kotkar and P. K. Ghosh, *Curr. Sci.*, 1988, **57**, 567.
- 35 V. Joshi and P. K. Ghosh, *J. Am. Chem. Soc.*, 1989, **111**, 5604.
- 36 P. V. Kamat, K. R. Gopidas, T. Mukherjee, V. Joshi, D. Kotkar, V. S. Pathak and P. K. Ghosh, *J. Phys. Chem.*, 1991, **95**, 10009.
- 37 N. Shimizu, S. Hashimoto, T. Takemura, M. Kawasaki and A. Yamagishi, in *Clays Controlling the Environment*, ed. G. J. Churchman, R. W. Fitzpatrick and R. A. Eggleton, Proceedings of the 10th International Clay Conference, CSIRO Publishing, Melbourne, 1995.
- 38 A. Awaluddin, R. N. Deguzman, C. V. Kumar, S. L. Suib, S. L. Burkett and M. E. Davis, *J. Phys. Chem.*, 1995, **99**, 9886.
- 39 R. A. Schoonheydt, in *Solid-State Supramolecular Chemistry: Two- and Three-Dimensional Inorganic Networks*, ed. G. Alberti, T. Bein, J. L. Atwood, J. E. D. Davies, D. MacNicol, F. Vögtle and J. M. Lehn, Elsevier Science Ltd., Oxford, 1996.
- 40 C. Breen, J. S. Brooks, S. Forder, A. A. Maggs, G. Marshall and G. R. Stephenson, *J. Mater. Chem.*, 1995, **5**, 97.
- 41 C. Breen, J. S. Brooks, S. Forder and J. C. E. Hamer, *J. Mater. Chem.*, 1996, **6**, 849.
- 42 A. VimondLaboudigue and R. Prost, *Clay Miner.*, 1995, **30**, 337.
- 43 J. F. Bank, G. Oforiokai and S. Bank, *Clays Clay Miner.*, 1993, **41**, 95.
- 44 J. M. Comets, V. Luca and L. Kevan, *J. Phys. Chem.*, 1992, **96**, 2645.
- 45 H. Sakane, M. O. Okabe and T. Suzuki, *J. Phys. IV (France)*, 1997, **7**, 1165.
- 46 J. D. Gale, A. K. Cheetham, R. A. Jackson, C. R. A. Catlow and J. M. Thomas, *Adv. Mater.*, 1990, **2**, 487.
- 47 D. J. Pruisen, P. Capkova, R. A. J. Driessen and H. Schenk, *Appl. Catal. A: Gen.*, 1997, **165**, 481.
- 48 P. Capkova, R. A. J. Driessen, H. Schenk and Z. Weiss, *J. Mol. Model.*, 1997, **3**, 467.
- 49 B. J. Teppen, K. Rasmussen, P. M. Bertsch, D. M. Miller and L. Schäfer, *J. Phys. Chem. B*, 1997, **101**, 1579.
- 50 B. J. Teppen, C. H. Yu, D. M. Miller and L. Schäfer, *J. Comput. Chem.*, 1998, **19**, 144.
- 51 H. Sato, A. Yamagishi and S. Kato, *J. Phys. Chem.*, 1992, **96**, 9377.
- 52 H. Sato, A. Yamagishi and S. Kato, *J. Am. Chem. Soc.*, 1992, **114**, 10933.
- 53 H. Sato, A. Yamagishi and S. Kato, *J. Phys. Chem.*, 1992, **96**, 9382.
- 54 H. Sato, A. Yamagishi, K. Naka and S. Kato, *J. Phys. Chem.*, 1996, **100**, 1711.
- 55 S. Park, A. Fitch and Y. L. Wang, *J. Phys. Chem. B*, 1997, **101**, 4889.
- 56 N. T. Skipper, F. R. C. Chang and G. Sposito, *Clays Clay Miner.*, 1995, **43**, 285.
- 57 J. Breu and K.-J. Range, *Monatsh. Chem.*, 1994, **125**, 141.
- 58 J. Breu, P. Belser and H. Yersin, *Acta Crystallogr., Sect. C*, 1996, **52**, 858.
- 59 J. Breu and A. J. Stoll, *Acta Crystallogr., Sect. C*, 1996, **52**, 1174.
- 60 Y. Masuda and H. Yamatera, *Bull. Chem. Soc. Jpn.*, 1984, **57**, 58.
- 61 M. Geringer, H. Gruber and H. Sterk, *J. Phys. Chem.*, 1991, **95**, 2525.
- 62 J. K. Thomas, *Acc. Chem. Res.*, 1988, **21**, 275.
- 63 D. R. Collins and C. R. A. Catlow, *Am. Mineral.*, 1992, **77**, 1172.
- 64 C. R. A. Catlow, R. G. Bell and J. D. Gale, *J. Mater. Chem.*, 1994, **4**, 781.
- 65 G. W. Watson, P. Tschaufeser, A. Wall, R. A. Jackson and S. C. Parker, in *Computer Modelling in Inorganic Crystallography*, ed. C. R. A. Catlow, Academic Press Inc., San Diego, 1997.
- 66 C. R. A. Catlow, L. Ackermann, R. G. Bell, F. Cora, D. H. Gay, M. A. Nygren, J. C. Pereira, G. Sastre, B. Slater and P. E. Sinclair, *Faraday Discuss.*, 1997, **106**, 1.
- 67 J. D. Gale, *Philos. Mag. B*, 1996, **73**, 3.
- 68 J. D. Gale, *J. Chem. Soc., Faraday Trans.*, 1997, **93**, 629.
- 69 P. P. Ewald, *Ann. Phys. (Leipzig)*, 1921, **64**, 253.
- 70 W. H. Press, S. A. Teukolsky, W. T. Vetterling and B. P. Flannery, *Numerical Recipes*, 2nd edn., Cambridge University Press, Cambridge, 1992.
- 71 A. Banerjee, N. Adams, J. Simons and R. Shepard, *J. Phys. Chem.*, 1986, **89**, 52.
- 72 B. G. Dick and A. W. Overhauser, *Phys. Rev.*, 1958, **112**, 90.
- 73 E. Sigfridsson and U. Ryde, *J. Comput. Chem.*, 1998, **19**, 377.
- 74 P. Grochowski, POL—Program for Derivation of Molecular Electrostatic Properties from DMOL DFT Calculations, Warsaw University, 1995.
- 75 F. L. Hirshfeld, *Theor. Chim. Acta*, 1977, **44**, 129.
- 76 B. Delley, *J. Chem. Phys.*, 1990, **92**, 508.
- 77 DMOL, MSI, 9658 Scranton Road, San Diego, CA 92121-2777, USA, 1996.
- 78 S. H. Vosko, L. Wilk and M. Nusair, *Can. J. Phys.*, 1980, **58**, 1200.
- 79 J. P. Perdew and Y. Wang, *Phys. Rev. B*, 1992, **45**, 13244.
- 80 A. D. Becke, *J. Chem. Phys.*, 1988, **88**, 2547.

- 81 D. P. Rillema and D. J. Jones, *J. Chem. Soc., Chem. Commun.*, 1979, 849.
- 82 D. P. Rillema, D. S. Jones, C. Woods and H. A. Levy, *Inorg. Chem.*, 1992, **31**, 2935.
- 83 M. Biner, H.-B. Bürgi, A. Ludi and C. Röhr, *J. Am. Chem. Soc.*, 1992, **114**, 5197.
- 84 J. M. Harrowfield and A. N. Sobolev, *Aust. J. Chem.*, 1994, **47**, 763.
- 85 E. Krausz, H. Riesen and A. D. Rae, *Aust. J. Chem.*, 1995, **48**, 929.
- 86 Molecular Simulation Program DISCOVER, MSI, 9658 Scranton Road, San Diego, CA 92121-2777, USA, 1996.
- 87 T. Oie, G. M. Maggiora, R. E. Christoffersen and D. J. Duchamp, *Int. J. Quantum Chem. Quantum Biol. Symp.*, 1981, **8**, 1.
- 88 J. B. Nicholas, F. R. Trouw, J. E. Mertz, L. E. Iton and A. J. Hopfinger, *J. Phys. Chem.*, 1993, **97**, 4149.
- 89 S. W. Bailey, in *Micas*, ed. S. W. Bailey and P. H. Ribbe, *Reviews in Mineralogy*, Mineralogical Society of America, Washington, D.C., 1984.
- 90 S. W. Bailey, *Clays Clay Miner.*, 1984, **32**, 81.
- 91 A. Pavese, G. Ferraris, M. Prencipe and R. Ibberson, *Eur. J. Mineral.*, 1997, **9**, 1183.
- 92 P. A. Schroeder and R. J. Pruett, *Am. Mineral.*, 1996, **81**, 26.
- 93 F. Muller, G. Besson, A. Manceau and V. A. Drits, *Phys. Chem. Miner.*, 1997, **24**, 159.
- 94 G. Lagaly, in *Layer Charge Characteristics of 2:1 Silicate Clay Minerals*, ed. A. R. Mermut, Clay Minerals Soc., Boulder, CO, 1994.
- 95 V. A. Drits, L. G. Dainyak, F. Muller, G. Besson and A. Manceau, *Clay Miner.*, 1997, **32**, 153.
- 96 J. D. Gale and N. J. Henson, *J. Chem. Soc., Faraday Trans.*, 1994, **90**, 3175.
- 97 R. A. Knurr and S. W. Bailey, *Clays Clay Miner.*, 1986, **34**, 7.
- 98 W. L. Jorgensen and D. L. Severance, *J. Am. Chem. Soc.*, 1990, **112**, 4768.
- 99 A. Gavezzotti, *Chem. Phys. Lett.*, 1989, **161**, 67.
- 100 G. R. Desiraju and A. Gavezzotti, *Acta Crystallogr., Sect. B*, 1989, **45**, 473.
- 101 C. A. Hunter, *Angew. Chem., Int. Ed. Engl.*, 1993, **32**, 1584.
- 102 C. A. Hunter, *Philos. Trans. R. Soc. London A*, 1993, **345**, 77.

Paper 8/09173K